Inorganic Chemistry

Article

pubs.acs.org/IC

# Ambient-Pressure Synthesis of Two New Vanadium-Based Calcium Ferrite-Type Compounds: $NaV_{1.25}Ti_{0.75}O_4$ and $NaVSnO_4$

Liliana Viciu,*[†] Alice Ryser,[†] Christian Mensing,[†] and Jan-Willem G. Bos[‡]

[†]Department of Chemistry and Applied Biosciences, ETH Zürich, Vladimir-Prelog-Weg 1, Zürich CH 8093, Switzerland

[‡]Institute of Chemical Sciences and Centre for Advanced Energy Storage and Recovery, School of Engineering and Physical Sciences, Heriot-Watt University, Edinburgh EH14 4AS, United Kingdom

**ABSTRACT:** Two new $CaFe_2O_4$-type compounds $NaV_{1.25}Ti_{0.75}O_4$ (**1**) and $NaVSnO_4$ (**2**) have been prepared at ambient pressure and temperatures < 800 °C. This contrasts with the parent material $NaV_2O_4$ which is synthesized at 6 GPa and 1300 °C. The lattice parameters are $a$ = 9.1500(4) Å, $b$ = 2.9399(3) Å, and $c$ = 10.6568(5) Å for **1** and $a$ = 9.3083(6) Å, $b$ = 3.0708(2) Å, and $c$ = 10.9194(5) Å for **2** (space group *Pnma*). Structure refinement against neutron powder diffraction data reveals that V/Ti and V/Sn are disordered over two octahedral sites. Both materials are characterized by a magnetic transition near 150 K below which the Curie moment is reduced from a value consistent with $V^{3+}$ [0.75 emu $mol_V^{-1}$ $K^{-1}$ for **1** and 0.58 emu $mol_V^{-1}$ $K^{-1}$ for **2**] to 0.23 emu $mol_V^{-1}$ $K^{-1}$ for **1** and 0.30 emu $mol_V^{-1}$ $K^{-1}$ for **2**, signaling a 70−50% reduction in the paramagnetic moment. The Weiss temperature ($\theta$) is reduced from −285 (**1**) and −138 K (**2**) to values close to 0 K, suggesting that the remaining spins are dilute and weakly interacting. Heat capacity measurements reveal a gradual loss of magnetic entropy between 2 and 150 K, consistent with short-range bulk magnetic ordering. In addition, heat capacity and magnetic susceptibility measurements reveal a number of weak magnetic transitions below 6 K involving both antiferromagnetic and ferromagnetic components.

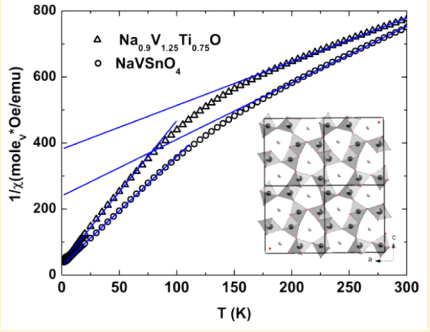


## 1. INTRODUCTION

The technological importance of functional materials has stimulated the search for synthetic approaches that afford the stabilization of compounds under comparatively benign conditions.[1,2] Thus, accessing high-temperature and high-pressure phases at more available conditions such as ambient pressure and/or low temperature are very important steps in materials synthesis. For example, neither $BiMnO_3$ nor $BiNiO_3$ can be obtained at ambient pressure.[3] However, a perovskite-type structure, $ABO_3$, with $Bi^{3+}$ on the A site was made at 1 atm by mixing $Mn^{4+}$ and $Ni^{2+}$ on the B site to give $BiMn_{2/3}Ni_{1/3}O_6$.[4] This was remarkable for the multiferroic field because it opened up a pathway for the synthesis at ambient pressure of magnetic and polar perovskites (other than $BiFeO_3$) by combining different ions on the B site.[5] Similarly, diluting the magnetism in the Laves phase, $NdFe_2$, by mixing Nd and Ce made the synthesis at ambient pressure of this phase possible.[6]

The peculiar architecture and chemical diversity of the calcium ferrite ($CaFe_2O_4$) structure suggests a field for intriguing physical properties.[7] In this structure type, zigzag chains of edge-shared octahedra ($FeO_6$) form pseudotriangular channels where the electropositive cation ($Ca^{2+}$) resides. The presence of triangular magnetic chains gives rise to geometric frustration and has resulted in complex magnetic behavior.[8,9] In the quasi-1D compound $CaV_2O_4$, two competing antiferromagnetic (AFM) interactions between $V^{3+}$ ions ($S$ = 1) were identified and result in magnetic frustration.[10,11] At temperatures between 108 and 145 K, a structural transition to a monoclinic phase (space group $P2_1/n$) occurs and removes the degeneracy between the exchange constants. An AFM transition then arises between $T_N \approx 51$ to 76 K. The temperature of both the structural phase transition and the magnetic ordering was found to be sample dependent.[11] $CaV_2O_4$ is an electrical insulator.[12] When $Ca^{2+}$ is replaced by $Na^+$ in $Ca_{1-x}Na_xV_2O_4$, complex magnetic behavior is observed with noncollinear AFM ordering and a metal to insulator transition for $x$ = 0.75 and 0.67.[13] When all the $Ca^{2+}$ ions are replaced with $Na^+$, the mixed valence of $V^{3.5+}$ results in metallic conductivity down to 40 mK that coexists with a noncollinear spin-density wave (SDW) AFM ordering below $T_N$ = 140 K.[14,15] As for many oxides of the calcium−ferrite family, only a high-pressure route yielded the desired $NaV_2O_4$ structure.

Here we report the synthesis at ambient pressure and characterization of $NaV_{1.25}Ti_{0.75}O_4$ (**1**) and $NaVSnO_4$ (**2**). Diluting the magnetic sublattice of $NaV_2O_4$ with Ti and Sn therefore affords $CaFe_2O_4$-type materials to be obtained at ambient pressure. Difficult synthetic conditions (1200 °C and a resistance furnace) are also used to get $NaTi_2O_4$ from Na metal and $TiO_2$,[16,17] although small crystals of $NaTi_2O_4$ were obtained from $Na_8Ti_5O_{14}$ and Ti at 770 °C using a KCl/NaCl flux.[18] Overall, the relatively soft conditions used here to obtain **1** and **2** are of interest. It has recently been demonstrated that $Na^+$ in $NaV_2O_4$ becomes mobile above

**Received:** March 25, 2015
**Published:** July 14, 2015




DOI: 10.1021/acs.inorgchem.5b00655
*Inorg. Chem.* 2015, 54, 7264−7271

250 K, offering possible application in electrochemical energy devices.[19] Therefore, we believe that the easy synthetic access to **1** and **2** demonstrated here is a remarkable step in fully exploiting the physical properties of these calcium ferrite-type compounds.

## 2. EXPERIMENTAL SECTION

The initial aim was to prepare $Na_2V_2(Ti/Sn)O_6$ honeycomb-type compounds similar to $Na_2Co_2TeO_6$ which some of us worked on previously.[20] The following starting materials were used: $Na_2CO_3$ (Fluka, >98.0%, annealed at 200 °C overnight to remove moisture), $V_2O_3$ (Sigma-Aldrich, 99%), $TiO_2$ nanopowder (ABCR), and $SnO_2$ (Sigma-Aldrich, 99.9%). In the preliminary reactions undertaken (0.5 g scale), the precursors were mixed in a Na:V:Ti(Sn) ratio of 2:2:1, pressed into pellets, and annealed under flowing nitrogen at 500 °C (2 days) and twice at 650 °C (2 × 2 days). The samples were contained in $Al_2O_3$ crucibles, and 10% excess $Na_2CO_3$ was added to compensate for loss due to volatilization. This led to the identification of $CaFe_2O_4$-type compounds for the Ti- and Sn-based compositions (Figure 1).

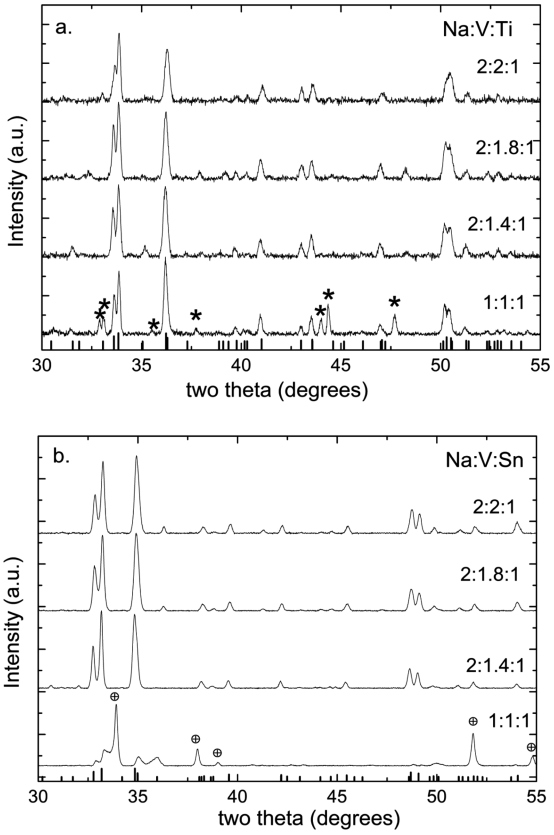


**Figure 1.** X-ray diffraction patterns of the products from reactions between varying ratios of (a) Na:V:Ti and (b) Na:V:Sn. Bragg reflection markers are for $NaV_{1.25}Ti_{0.25}O_4$ and $NaVSnO_4$. Peaks marked with an asterisk (*) correspond to Na−V−O phases (i.e., $NaVO_3$, $Na_2V_2O_5$, and $Na_3VO_4$), and peaks marked with a "circled +" correspond to $SnO_2$.

Attempts to form $CaFe_2O_4$-type compounds (i.e., $NaVTiO_4$ and $NaVSnO_4$) from a 1:1:1 ratio of the starting materials led to the observation of increased amounts of impurities, including Na−V−O phases ($NaVO_3$, $Na_2V_2O_5$, and $Na_3VO_4$) for Ti and $SnO_2$ for Sn (Figure 1). The Na:V:Ti(Sn) ratio was subsequently varied, and ratios of 2:1.8:1 and 2:1.4:1 were tried with the latter giving the best sample purities (Figure 1). After these preliminary steps the synthesis conditions were optimized, and the following conditions were used to prepare **1** and **2** (0.5 g scale): The first heating step was 2 days at 650 °C followed by homogenization using a mortar and pestle and subsequent heating for 3 days at 700 °C ($NaV_{1.25}Ti_{0.75}O_4$) and for 3 days at 750 °C ($NaVSnO_4$), with one intermediate grinding in each case. All steps were done under a $N_2$ atmosphere. The furnace ramp rates were 150 °C/h upon heating and cooling. A starting temperature higher than 650 °C resulted in a melt where the material poured through the crucible pores, while a final temperature higher than 750 °C resulted in a larger number of impurities. The obtained black powders were checked for purity by X-ray powder diffraction (XRD) using a STOE diffractometer with monochromated Cu $K\alpha_1$ radiation. Neutron powder diffraction (NPD) data were collected on 2 g samples at the Institut Laue Langevin (France) on the super-D2B diffractometer with neutrons of wavelength 1.594 Å over the range from 10° to 155° with a 0.05° step size. The NPD sample for compound **2** contained a substantial amount of unreacted $V_2O_3$ that was not present in the smaller sample used for the physical property measurements. Rietveld refinement was performed using the GSAS suite of programs.[21] The magnetic properties were investigated with a Quantum Design Magnetic Property Measurement System. Zero-field-cooled (ZFC) and field-cooled (FC) magnetization data were taken between 2 and 300 K in applied magnetic fields of 0.01 and 1 T. Field-dependent magnetization data were recorded at 2 and 5 K for **1** and at 2, 5, and 10 K for **2**. Alternating current susceptibility measurements were recorded using the Quantum Design Physical Properties Measurement System (PPMS) AC/DC magnetometer option with an ac drive field of 10 Oe, oscillating at 0.1, 2.5, 5.0, and 10.0 kHz for **1** and 0.01, 5.0, and 10.0 kHz for **2**. The heat capacity was measured between 1.9 and 20 K using the heat capacity option of the PPMS. The isostructural nonmagnetic $NaScTiO_4$ sample was prepared as described elsewhere and used to extract the lattice contribution to the specific heat of the title compounds.[22]

## 3. RESULTS

**3.1. Crystal Structure.** The synthesis procedure has been described in the Experimental Section, and the most striking feature is that excess Na and V are needed for successful formation of **1** and **2**. This will be discussed after determination of the experimental compositions of **1** and **2** from neutron powder diffraction.

The NPD data collected on **1** and **2** were indexed with an orthorhombic unit cell in the space group *Pnma* (No. 62). The unit cell parameters of the new compounds and reported values for $NaV_2O_4$ and $NaTi_2O_4$ are presented in Table 1. This reveals that the lattice parameters for **1** fall in between those for $NaV_2O_4$ and $NaTi_2O_4$, while **2** has a substantially increased unit cell volume, consistent with the larger size of $Sn^{4+}$ ($r_{V3+}$= 0.78 Å, $r_{Ti4+}$ = 0.745 Å; $r_{Sn4+}$ = 0.83 Å),[23] and the cell metrics of $NaFeSnO_4$ (Table 1). The initial structural model was based on $CaFe_2O_4$, in which Na replaces Ca, while V and Ti(Sn) occupy the Fe sites.[24] This model readily converged and gave a good quality of fit. The final Rietveld fits are shown in Figure 2a and 2b, and the fitted atomic positions, thermal displacement parameters, and fit statistics are listed in Table 2. The refined stoichiometry of the compounds is $Na_{0.97(1)}V_{1.23(2)}Ti_{0.77(2)}O_4$ and $Na_{0.98(2)}V_{1.04(2)}Sn_{0.96(2)}O_4$. A simplified notation of $NaV_{1.25}Ti_{0.75}O_4$ (**1**) and $NaVSnO_4$ (**2**) is used throughout the paper. Table 3 contains a selection of bond distances and angles, while a polyhedral representation of the structure is given in Figure 3. It was necessary to restrain the thermal displacement parameters for both samples as free refinement led to small values for the M1 and M2 sites, but this likely reflects the difficulty in identifying a correct background and does not affect the refined compositions. The linearly decreasing background for **2** suggests the presence of a substantial amorphous phase, while this sample also contains 9.7(1) wt % of unreacted $V_2O_3$. Please note that both **1** and **2**


DOI: 10.1021/acs.inorgchem.5b00655
*Inorg. Chem.* 2015, 54, 7264−7271

**Table 1. Lattice Parameters for $NaV_{1.25}Ti_{0.75}O_4$ and $NaVSnO_4$ from Neutron Diffraction Analysis[a]**

| compound | $a$ (Å) | $b$ (Å) | $c$ (Å) | $V$ (Å$^3$) | ref |
|---|---|---|---|---|---|
| $NaTi_2O_4$ | 9.262(1) | 2.9556(3) | 10.7537(7) | 294.36(5) | 14 |
| $NaV_{1.25}Ti_{0.75}O_4$ | 9.1500(4) | 2.9399(2) | 10.6568(5) | 286.67(3) | this work |
| $NaV_2O_4$ | 9.130(1) | 2.8844(4) | 10.628(1) | 279.91(6) | 12 |
| $NaVSnO_4$ | 9.3083(6) | 3.0708(2) | 10.9194(6) | 312.12(3) | this work |
| $NaFeSnO_4$ | 9.331(4) | 10.970(5) | 3.060(1) | 313.2(1) | 24 |

[a]Space group *Pnma* (No. 62). Cell parameters and volume for the isostructural $NaV_2O_4$, $NaTi_2O_4$, and $NaFeSnO_4$ are shown for comparison.

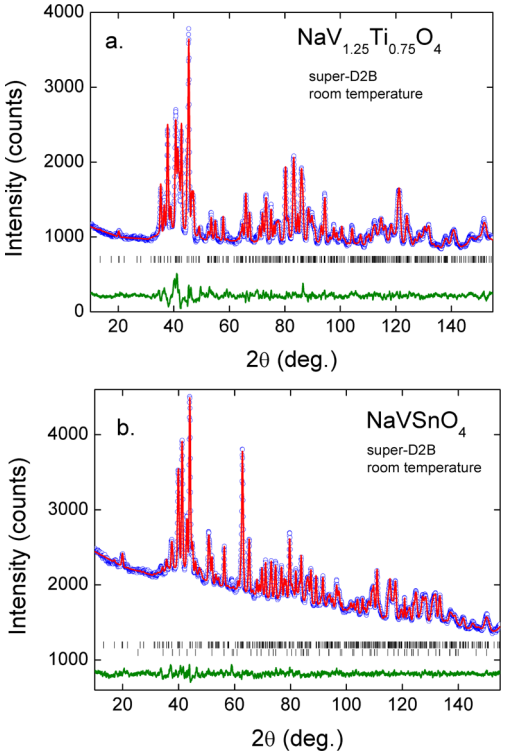


**Figure 2.** Observed (open circles), calculated (solid red line), and difference Rietveld profiles for fits to super-D2B neutron powder diffraction data collected on (a) $NaV_{1.25}Ti_{0.75}O_4$ and (b) $NaVSnO_4$. Markers correspond to the Bragg positions for the main $CaFe_2O_4$-type phase (top line) and a 10 wt % unreacted $V_2O_3$ phase (bottom line) in the $NaVSnO_4$ sample.

**Table 2. Structural Parameters for $NaV_{1.25}Ti_{0.75}O_4$ and $NaVSnO_4$ at Room Temperature[a]**

| | | $NaV_{1.25}Ti_{0.75}O_4$ | $NaVSnO_4$ |
|---|---|---|---|
| Na | $x$ | 0.2445(6) | 0.2448(5) |
| | $z$ | 0.3503(6) | 0.3471(6) |
| | $U_{iso}$ (Å$^2$) | 0.0057(5) | 0.0047(3) |
| | Occ. | 0.97(1) | 0.98(2) |
| M1 | $x$ | 0.065(1) | 0.0663(7) |
| | $z$ | 0.109(1) | 0.1132(5) |
| | $U_{iso}$ (Å$^2$) | 0.0057(5) | 0.0047(3) |
| | Occ. | V/Ti 0.55(1)/0.45(1) | V/Sn 0.56(1)/0.44(1) |
| M2 | $x$ | 0.080(2) | 0.0842(6) |
| | $z$ | 0.604(1) | 0.6075(4) |
| | $U_{iso}$ (Å$^2$) | 0.0057(5) | 0.0047(3) |
| | Occ. | V/Ti 0.68(1)/0.32(1) | V/Sn 0.48(1)/0.52(1) |
| O1 | $x$ | 0.2892(4) | 0.2924(3) |
| | $z$ | 0.6480(3) | 0.6533(3) |
| | $U_{iso}$ (Å$^2$) | 0.0057(5) | 0.0047(3) |
| O2 | $x$ | 0.3876(4) | 0.3840(3) |
| | $z$ | 0.9793(3) | 0.9818(3) |
| | $U_{iso}$ (Å$^2$) | 0.0057(5) | 0.0047(4) |
| O3 | $x$ | 0.4789(4) | 0.4781(3) |
| | $z$ | 0.2173(3) | 0.2171(2) |
| | $U_{iso}$ (Å$^2$) | 0.0057(5) | 0.0047(4) |
| O4 | $x$ | 0.0758(4) | 0.0762(3) |
| | $z$ | 0.9274(3) | 0.9272(2) |
| | $U_{iso}$ (Å$^2$) | 0.0057(5) | 0.0047(4) |
| | wRp (%) | 4.0 | 1.4 |
| | Rp (%) | 2.8 | 1.1 |
| | $\chi^2$ | 10.5 | 3.2 |

[a]Space group: *Pnma* (No. 62). All atoms are in site 4*c* ($x$, 1/4, $z$).

also contain Na−V−O phases, in particular $NaVO_3$, which is readily identified in X-ray diffraction (e.g., 8 wt % for **1**) but only results in weak reflections in the neutron data.

The structures of **1** and **2** contain double rows of edge-sharing $(M)O_6$ octahedra which run along the *b* axis and share corners to enclose a pseudotriangular channel which is occupied by the $Na^+$ ions (Figure 3a). Within the double chains the M cations have an edge-sharing triangular arrangement, leading to the potential for magnetic frustration (Figure 3b and 3c). There are two types of double chains: the first contains the M1 site, while the second contains the M2 cations (Table 1 and Figure 3). The shortest M−M distances are equal to the *b* axis (2.94 Å for **1** and 3.07 Å for **2**), while the diagonal distances are 3.00 (M1−M1) and 3.08 Å (M2−M2) for **1** and 3.16 (M1−M1) and 3.21 Å (M2−M1) for **2**, respectively. These distances are short enough to support direct bonding between the metals. There are two slightly longer interchain M1−M2 distances, and these metals are separated by an oxygen anion. The first, along the *a* axis, is 3.56 Å for **1** and 3.59 Å for **2**, and the second, along the *c* axis, is 3.64 Å for **1** and 3.69 Å for **2**. The $MO_6$ octahedra are slightly distorted, but this is common for this class of materials. Defining the distortion factor as the ratio between the longest and the shortest bond gives values of 1.05 (M1) and 1.03 (M2) for **1** and 1.02 (M1) and 1.05 (M2) for **2**. Similar distortions were observed in $NaV_2O_4$ and $NaTi_2O_4$ where the site-averaged distortion factors are 1.02 and 1.04, respectively.[14,17] The distortion ratios for $NaScSnO_4$ and $NaFeSnO_4$ are 1.03 and 1.02, respectively.[22] The M($n$)−O−M($n$) angles within the double chains range from 93° to 100° for **1** and from 95° to 100° for **2**. The M1−O−M2 angles between the chains are 126.4° and 131.7° for **1** and 124.2° and 130.9° for **2**. The local moment magnetism discussed below suggests that superexchange may be an important factor in addition to the direct bonding between the M centers, and the observed M−O−M angles suggest a mixture of ferromagnetic (FM) and AFM interactions. The oxidation state of vanadium is expected to be +3.3 for **1** based on the refined stoichiometry and +3 for **2**. The bond valence parameters for $V^{3+}$ and $Ti^{4+}$ are almost identical,[25] and bond valence sums (BVS) of 3.33 (M1) and 3.44 (M2) were


DOI: 10.1021/acs.inorgchem.5b00655
*Inorg. Chem.* 2015, 54, 7264−7271

**Table 3. Selected Bond Distances, Bond Valence Sums, and Bond Angles for $NaV_{1.25}Ti_{0.75}O_4$ and $NaVSnO_4$**

| | $NaV_{1.25}Ti_{0.75}O_4$ | $NaVSnO_4$ |
|---|---|---|
| bond distances (Å) | | |
| M1−O1 (2×) | 2.027(8) | 2.069(5) |
| M1−O3 (1×) | 2.01(1) | 2.026(7) |
| M1−O4 (2×) | 1.995(8) | 2.076(5) |
| M1−O4 (1×) | 1.94(1) | 2.033(6) |
| **average bond** | **1.99 (1)** | **2.058(9)** |
| average bond in $NaV_2O4$ (V1−O) | 1.972 | |
| average bond in $NaTi_2O4$ (Ti1−O) | 2.025 | |
| **BVS** | **3.33** | **3.4** |
| M2−O1 (1×) | 1.96(2) | 2.001(6) |
| M2−O2 (2×) | 2.014(9) | 2.081(4) |
| M2−O2 (1×) | 1.99(2) | 2.103(6) |
| M2−O3 (2×) | 1.97(1) | 2.031(3) |
| **average bond** | **1.986(9)** | **2.05(1)** |
| average bond in $NaV_2O_4$ | 1.981 | |
| average bond in $NaTi_2O_4$ | 2.002 | |
| **BVS** | **3.44** | **2.975** |
| M1−M1 (×2) | 2.9407(2) | 3.0711(1) |
| M1−M1 (×2) | 3.00(2) | 3.16 (1) |
| M2−M2 (×2) | 2.9407(2) | 3.0711(1) |
| M2−M2 (×2) | 3.08(3) | 3.21(1) |
| M1−M2 (×2) | 3.56(2) | 3.598(8) |
| M1−M2 (×2) | 3.64(2) | 3.690(6) |
| bond angles (deg) | | |
| M1−O1−M1 (×1) | 93.0(5) | 95.8(3) |
| M1−O4−M1 (×2) | 99.4(4) | 100.6(2) |
| M1−O4−M1 (×1) | 95.0(5) | 95.4(3) |
| M2−O2−M2 (×1) | 93.8(6) | 95.1(2) |
| M2−O2−M2 (×2) | 100.3(5) | 100.4(2) |
| M2−O3−M2 (×1) | 96.5(6) | 98.2(2) |
| M1−O1−M2 (×2) | 126.4(4) | 124.2(2) |
| M1−O3−M2 (×2) | 131.7(3) | 130.9(1) |

calculated for **1**. These values are in good agreement with the average nominal charge per transition metal (+3.5). The BVS calculation for **2** used an average bond valence parameter (1.78 for V and 1.905 V for Sn) which yielded sums of 3.4 (M1) and 3.0 (M2), in reasonable agreement with the expected charge.

Inspection of Figure 1 reveals variations in cell parameters as the ratio of the reactants is changed, suggesting that a degree of $NaV_{2-x}Ti_xO_4$ and $NaV_{2-x}Sn_xO_4$ solid solution formation occurs. The cell volumes of **1** and **2** and the known end members (Table 1) are plotted in Figure 4, enabling an

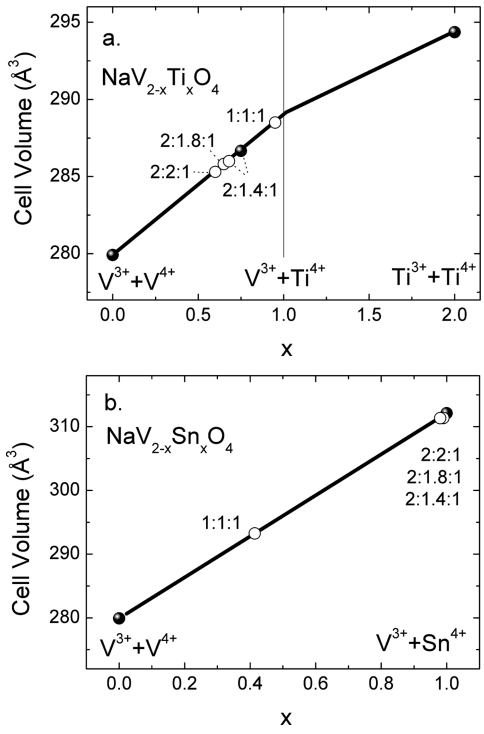


**Figure 4.** Composition dependence of the unit cell volume for the (a) $NaV_{2-x}Ti_xO_4$ and (b) $NaV_{2-x}Sn_xO_4$ series. Solid black circles are known compositions from this study and from the literature (see Table 1). Open circles correspond to the cell volumes of samples prepared at different starting ratios, where linear interpolation between known compositions has been used to estimate the composition (see text). An indication of the expected oxidation states is also given.

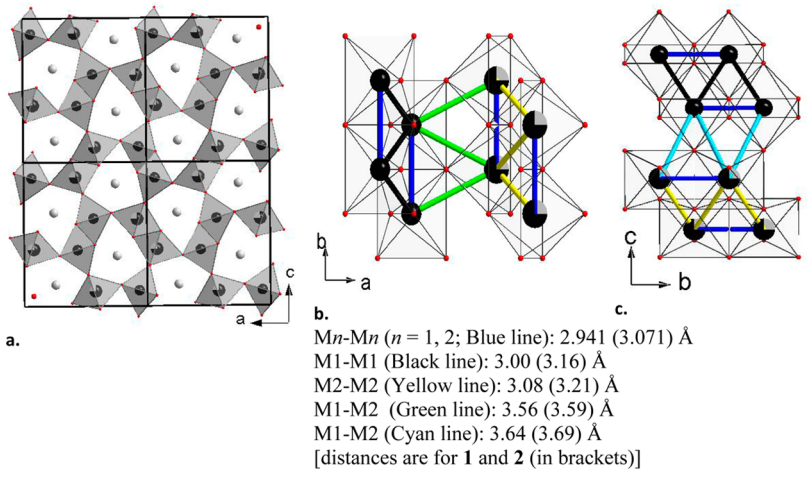


**Figure 3.** Schematic representation of the $CaFe_2O_4$-type crystal structure. (a) View along the *b* axis: The transition metals (M1, black spheres; M2, black octants) are octahedrally coordinated by oxygen. Na ions, shown in gray, are found inside the channels formed by the $MO_6$ double chains. (b) View along the *c* axis: Infinite columns of double rows of edge-shared $MO_6$ octahedra run parallel to the *b* axis. Each double row is made of one crystallographic site, M1 and M2. (c) View of the double chains along the *a* axis.



DOI: 10.1021/acs.inorgchem.5b00655
*Inorg. Chem.* 2015, 54, 7264−7271

estimate of the range of compositions that can be obtained by variation of the starting composition. $NaV_2O_4$ ($x = 0$) contains a 1:1 mixture of $V^{3+}$ and $V^{4+}$, and it is reasonable to expect that $V^{4+}$ is replaced by $Ti^{4+}/Sn^{4+}$, followed by replacement of $V^{3+}$ by $Ti^{3+}$, while further substitution of $Sn^{4+}$ is not possible, unless $V^{2+}$ is stabilized. The presence of either $Ti^{3+}$ or $V^{2+}$ is doubtful under the mildly reducing atmospheres and moderate temperatures employed, suggesting an upper limit of $x = 1$ for the samples studied here. The presence of two substitution regimes is supported by the data on the $NaV_{2-x}Ti_xO_4$ series which do not follow a linear interpolation between the end members (see Figure 4a). Due to the paucity of data points we assumed two linear regimes with the crossover point at $x = 1$. This enables us to estimate the compositions for the other starting ratios as follows: $x = 0.60$ (2:2:1; $x_{nominal} = 0.67$), 0.65 (2:1.8:1; $x_{nominal} = 0.71$), 0.68 and 0.75 (2:1.4:1; $x_{nominal} = 0.83$), and 0.95 (1:1:1; $x_{nominal} = 1$), indicating a solubility range of $0.60 \leq x \leq 0.95$ for the Ti-substituted samples. Here, the $x_{nominal}$ values have been calculated from the V:Ti ratio in the starting mixture. The experimental compositions therefore follow the V:Ti ratio in the starting mixture reasonably closely. In the case of the $NaV_{2-x}Sn_xO_4$ series, the 2:2:1−2:1.4:1 starting ratios ($0.67 \leq x_{nominal} \leq 0.8$) all yield experimental values close to $x = 1$ (Figure 4b). The exception is the 1:1:1 sample, which contains a small amount of a $CaFe_2O_4$-type phase with a cell volume consistent with $x = 0.41$ (Figures 1 and 4). One of the most striking observations is therefore that the 1:1:1 starting composition yields the least pure samples for both series. For the Ti 1:1:1 reaction, $NaVO_3$, $Na_2V_2O_5$, and $Na_3VO_4$ are observed in the XRD data, while a large amount of unreacted $SnO_2$ is evident for the 1:1:1 Sn sample. The key difference is that the 1:1:1 Ti reaction yields $x = 0.92$, which is close to that expected ($x = 1$), whereas the $CaFe_2O_4$ phase for the 1:1:1 Sn sample has $x = 0.4$, consistent with the observed presence of unreacted $SnO_2$. The starting compositions that lead to better quality samples are rich in Na and V (Figure 1), suggesting that low melting point Na−V−O phases are present and improve the reaction kinetics. The most commonly observed phase is $NaVO_3$, which has a melting point of 630 °C. Complete identification of the Na−V−O phases present is difficult due to the often low symmetries and weak XRD reflections. The improved sample quality for the 2:2:1−2:1.4:1 starting ratios occurs because the flux phases do not compete with the formation of the $CaFe_2O_4$-type phase by reducing the amount of V available. This leads to improved yields but in the presence of residual Na−V−O phases.

**3.2. Magnetism.** The high-pressure phase $NaV_2O_4$ is metallic from resistivity and heat capacity measurements and has an incommensurate AFM spin density wave transition at 140 K. Despite the itinerant nature of the charge transport, the magnetism is Curie−Weiss type with paramagnetic moments typical for a mixture of spin-only $V^{3+}$ ($S = 1$) and $V^{4+}$ ($S = 1/2$). The structural analysis described above reveals that **1** and **2** have a diluted magnetic sublattice, and that the oxidation state of V is pushed toward +3. For **1**, the M1 site is almost equally (55/45) occupied by V/Ti, while the M2 site has a 70/30 V/Ti occupancy. For **2**, both M1 and M2 sites are approximately 50% occupied by Sn. The experimental inverse magnetic susceptibilities (main panels) and the low-temperature susceptibilities (insets) for **1** and **2** are shown in Figure 5a and 5b. The inverse susceptibilities evidence two Curie−Weiss regimes with a transition near 150 K. The fitted high-temperature (170−300 K) Curie constants ($C$) and Weiss

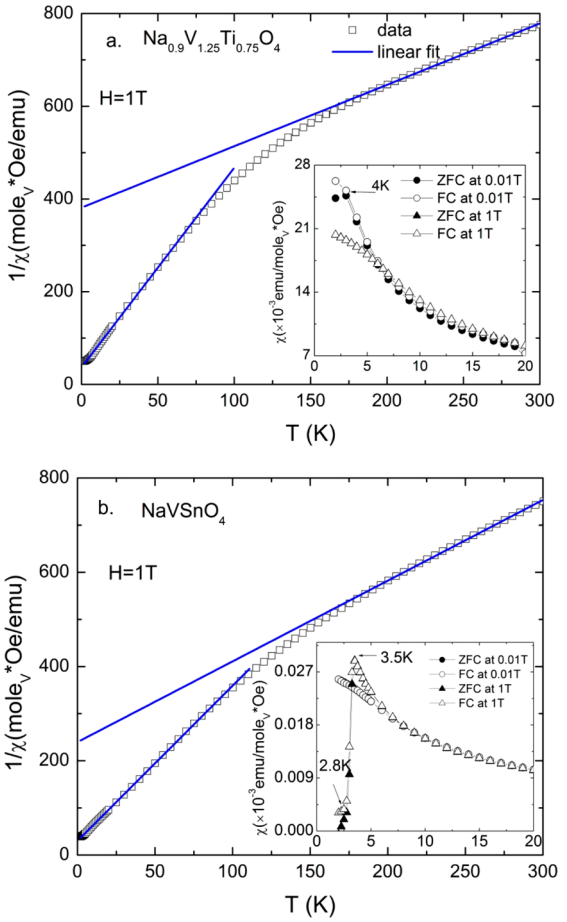


**Figure 5.** Temperature dependence of the inverse magnetic susceptibility for (a) $NaV_{1.25}Ti_{0.75}O_4$ and (b) $NaVSnO_4$; blue lines are fits to the Curie−Weiss law (see text). (Insets) Magnetic transitions at low temperatures.

temperatures ($\theta$) are $C = 0.75$ emu $mol_V^{-1}$ $K^{-1}$ and $\theta = -285$ K for **1** and $C = 0.58$ emu $mol_V^{-1}$ $K^{-1}$ and $\theta = -138$ K for **2.** The fitted low-temperature (5−75 K) values are $C = 0.23$ emu $mol_V^{-1}$ $K^{-1}$ and $\theta = -7.8$ K for **1** and $C = 0.30$ emu $mol_V^{-1}$ $K^{-1}$ and $\theta = -9$ K for **2**. The samples therefore lose about 70−50% of their Curie moment below 150 K. This temperature closely coincides with the SDW ordering temperature in $NaV_2O_4$. The absence of a sharp ordering transition suggests that our randomly diluted magnetic sublattices exhibit short-range AFM order. This is supported by the large reduction in Weiss temperature ($\theta$ < 10 K below 75 K), suggesting that the remaining residual spins are well separated and do not interact very strongly. The larger fraction of remaining paramagnetic spins for **2** is in keeping with the larger magnetic dilution for that compound. The calculated paramagnetic moments are 2.5 (**1**) and 2.2 $\mu_B$ (**2**) in the high-temperature regime and decrease to 1.4 and 1.6 $\mu_B$ in the low-temperature domain. The expected spin-only value for $V^{3+}$ ($S = 1$) is 2.82 $\mu_B$, which is close to the observed experimental high-temperature values. Better agreement can be obtained for **1** by assuming a mixture of 0.25 $V^{4+}$ ($S = 1/2$) and 1 $V^{3+}$, which yields a spin-only moment of 2.65 $\mu_B$. The low field magnetic susceptibilities evidence AFM transitions that are readily suppressed in an applied field of 1 T (insets to Figure 5a and 5b), lending further support for the weakly interacting dilute nature of the residual spins. The field dependence of the magnetization for **1** and **2** at low


DOI: 10.1021/acs.inorgchem.5b00655
Inorg. Chem. 2015, 54, 7264−7271

temperatures is shown in Figure 6a and 6b. Both samples show a small magnetic hysteresis at 2 K (insets to Figure 6a and 6b),

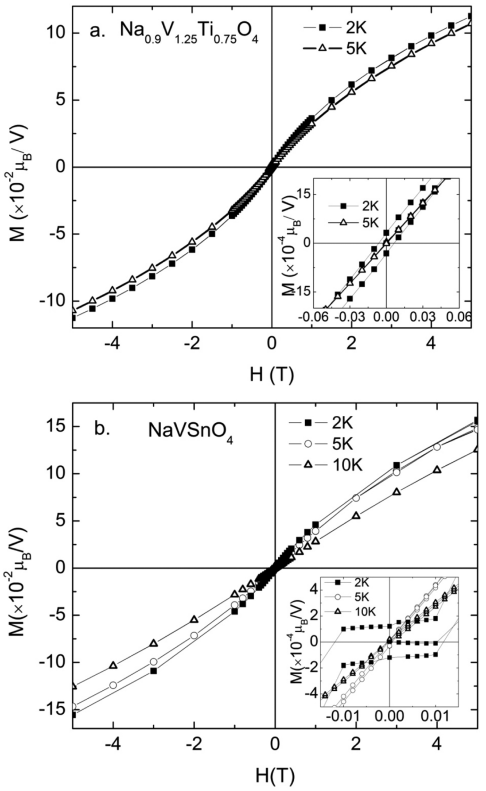


**Figure 6.** Field dependence of the magnetization at 2 and 5 K for $NaV_{1.25}Ti_{0.75}O_4$ (a) and at 2, 5, and 10 K for $NaVSnO_4$ (b). (Insets) Magnetic hysteresis at low temperature.

indicating weak FM interactions, while this disappears at 5 K, and the magnetization remains Brillouin like. The low-temperature magnetic transitions were further probed using ac susceptibility measurements which are shown in Figure 7a and 7b. For **1**, M′ shows a broad AFM transition with a maximum at $T_m'$ = 5.75 K (Figure 7a). This maximum occurs at a temperature somewhat higher than in the dc data ($T_m$ = 4 K). There is no frequency dependence of $T_m'$, and there is no signature of a spin-glass transition. In the imaginary component, M″, a sharper transition is apparent at $T_m'$ = 5.38 K. For **2** the dc and M′ data are in good agreement (Figure 7b) with a sharp AFM transition at $T_m'$ = 4 K ($T_m$ = 3.5 K). In the imaginary part (M″) the transition at 4 K is absent and only a small cusp appears at $T_m'$ = 2.9 K, which corresponds to the slight divergence at 2.8 K seen in the dc measurements.

**3.3. Heat Capacity.** The temperature dependence of the heat capacity ($C_p$) of compounds **1** and **2** and the nonmagnetic analogue $NaScTiO_4$ are shown in Figure 8a. The data for the reference sample was corrected for the difference in formula weight and scaled at high temperatures, so that an estimate of the magnetic contribution to the heat capacity can be made. No transitions were evident near 150 K. The inset shows the low-temperature behavior of $C_p/T$ which reveals the presence of two broad anomalies at temperatures consistent with the transitions observed in the magnetic susceptibility data (4 K for **1** and 3.5 K for **2**). The magnetic contribution to the heat capacity was obtained by subtraction of the lattice contribution

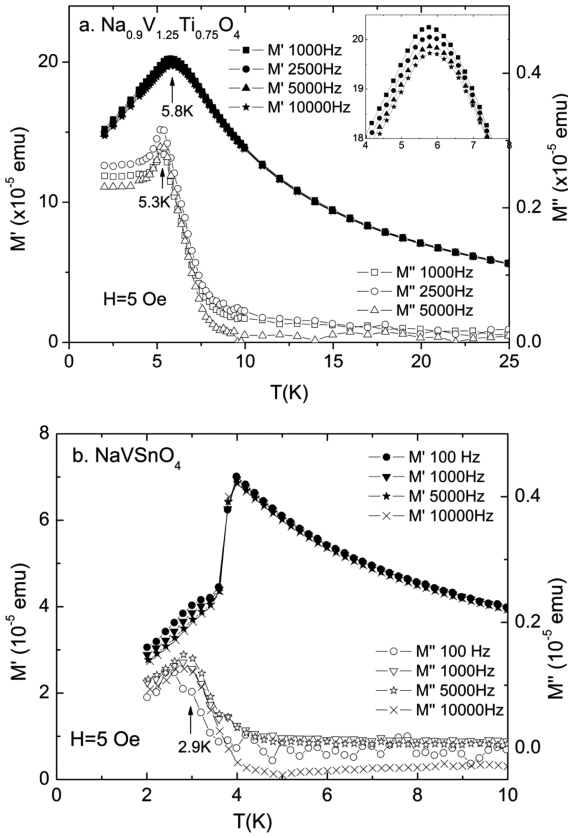


**Figure 7.** Temperature dependence of the real (M′) and imaginary (M″) components of the alternating current (ac) magnetization for (a) $NaV_{1.25}Ti_{0.25}O_4$ and (b) $NaVSnO_4$.

of the diamagnetic analogue and is plotted as $\Delta C_p/T$ in Figure 8b. This reveals extremely broad features for both samples with maxima between 25 and 50 K, as well as the low-temperature transitions that were already evident from Figure 8a. Integration of the $\Delta C_p/T$ data yields magnetic entropies of 10.3 and 9.7 J mol$^{-1}$ K$^{-1}$ for **1** and **2**, respectively. These values are in good agreement with the calculated $[R\ln(2S + 1)]$ values of 10.5 (mixed $S$ = 1 and 1/2 system) and 9.1 J mol$^{-1}$ K$^{-1}$ for **2** ($S$ = 1). The temperature dependence of the magnetic entropy is shown in Figure 8c. This reveals a rapid release of magnetic entropy up to 50 K (~90% of the total recovered) and no further significant increase above 100 K. Despite the uncertainty caused by the presence of the Na−V−O phases in these samples, this clearly demonstrates that the reduction in Curie moment observed in the susceptibility data is a bulk effect. The broad nature of the magnetic transition suggests that the AFM ordering is extremely short ranged and perhaps even dynamic.

## 4. DISCUSSION

Two new $CaFe_2O_4$-type compositions, $NaV_{1.25}Ti_{0.75}O_4$ (**1**) and $NaVSnO_4$ (**2**), were successfully synthesized at ambient pressure and 700−750 °C under a nitrogen atmosphere. This contrasts with the synthesis of $NaV_2O_4$ at high pressure and 1500 °C and of $NaTi_2O_4$ which was obtained by reacting metallic Na with $TiO_2$.[16] The samples were obtained using an optimized Na:V:Ti(Sn) = 2:1.4:1 starting ratio. Any attempts to move the starting composition closer to the compositions obtained from neutron powder diffraction led to samples of poorer phase purity. However, the data do demonstrate a


DOI: 10.1021/acs.inorgchem.5b00655
Inorg. Chem. 2015, 54, 7264−7271

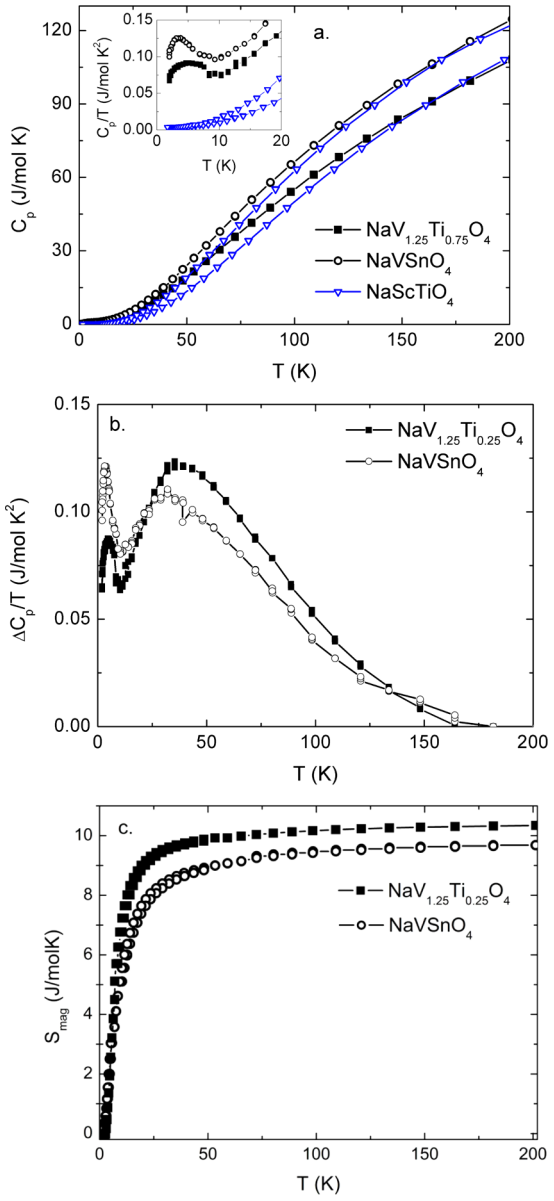


**Figure 8.** (a) Temperature dependence of the heat capacity ($C_p$) for $NaV_{1.25}Ti_{0.75}O_4$ and $NaVSnO_4$, as well as the nonmagnetic analogue $NaScTiO_4$. Data for $NaScTiO_4$ were corrected for weight difference and scaled to match the data above 175 K. (Inset) Low-temperature behavior of $C_p/T$. (b) Magnetic contribution to the heat capacity plotted as $\Delta C_p/T$ versus temperature. (c) Temperature evolution of the magnetic entropy ($S_{mag}$).

considerable degree of solid solution formation. For $NaV_{2-x}Ti_xO_4$, values between $0.6 \leq x \leq 0.95$ were observed, while the observation of a minor phase with $x = 0.41$ for $NaV_{2-x}Sn_xO_4$ suggests that this series also exists over a wider interval. In both cases, the experimental compositions imply an upper limit of $x = 1$ (Figure 4), which is consistent with the mild reducing conditions and the need to stabilize $Ti^{3+}$ or $V^{2+}$ for $x > 1$. The apparent necessity for an excess of Na and V suggests low melting point Na−V−O phases, including $NaVO_3$, serve as a flux that speeds up the reaction. This is reminiscent of, e.g., the NaCl−KCl eutectics that were used to obtain $NaTi_2O_4$ from $Na_8Ti_5O_{14}$ and Ti at moderate temperatures.[18] Further improvements in synthesis methodology are needed to obtain phase-pure samples, but these results demonstrate that $CaFe_2O_4$-type compounds can be obtained using the relatively benign conditions used here. The crystal structure of **1** and **2** contains double chains of edge-sharing $MO_6$ octahedra. This leads to a geometrically frustrated arrangement of the M cations (Figure 3). For the samples presented here, the M1 double chains are diluted by 50% for both compositions, while the M2 chain is 30% diluted for **1** (Ti) and 50% diluted for **2** (Sn). The average magnetic dilution is 37.5% for **1** and 50% for **2**. The magnetic susceptibilities clearly evidence a reduction in Curie paramagnetic moment below 150 K, which is consistent with AFM ordering of the majority of the spins, leaving a small fraction of weakly interacting residual spins. In both cases, a very small magnetic hysteresis is observed suggesting the presence of a FM component to the interactions between the dilute spins. The heat capacity results are consistent with short-range AFM ordering, and the large recovered magnetic entropies reveal that this is a bulk effect. Similar broad magnetic contributions to the heat capacity and dilute low-temperature magnetism were observed in ordered $A_2YMoO_6$ double perovskites, where the majority of $S = 1/2$ spins forms a valence bond glass at ∼150 K, while a small fraction of residual paramagnetic spins shows a spin-glass transition at $T < 2$ K for A = Ba,[26] whereas for A = Sr a FM transition is observed at 10 K.[27]

## 5. CONCLUSIONS

Two new $CaFe_2O_4$-type compounds, $NaV_{1.25}Ti_{0.75}O_4$ and $NaVSnO_4$, are reported, and their crystal structures were refined from powder neutron diffraction. They are obtained at ambient pressure and relatively low temperature (650−700 °C) unlike the isostructural $NaV_2O_4$ which is prepared at high temperature (>1300 °C) and high pressure (6 GPa). The more benign synthetic conditions are attributed to the presence of low-melting point Na−V−O phases in the reaction mixture that serve to improve the kinetics. This makes $CaFe_2O_4$ structures containing Na and V more accessible and their exploration in fields such as batteries or materials with peculiar magnetism more appealing. Further work, including the growth of single crystals of both compounds, would be of interest in studying the magnetic structure and the transport properties.

## AUTHOR INFORMATION


### Corresponding Author

*E-mail: viciuma@ethz.ch.


### Notes

The authors declare no competing financial interest.


Email address for J.-W.G.B.: j.w.g.bos@hw.ac.uk.


## ACKNOWLEDGMENTS


L.V. gratefully acknowledges Prof. Reinhard Nesper and Laboratory of Inorganic Chemistry at ETH Zurich for the infrastructure and financial support.


## REFERENCES


(1) Jansen, M.; Schon, J. C. *Compr. Inorg. Chem. II* **2013**, *9*, 941−969.

(2) Wang, Z. L.; Kang, Z. C. *Functional and Smart Materials: Structural Evolution and Structure Analysis*, 1st ed.; Plenum Press: New York, 1998; ISBN: 0306456516.

(3) Ishiwata, S.; Azuma, M.; Takano, M.; Nishibori, E.; Takata, M.; Sakata, M.; Kato, K. *J. Mater. Chem.* **2002**, *12*, 3733−7. Belik, A. A.; Kodama, K.; Naoki Igawa, N.; Shamoto, S.; Kosuda, K.; Takayama-Muromachi, E. *J. Am. Chem. Soc.* **2010**, *132*, 8137−8144.




DOI: 10.1021/acs.inorgchem.5b00655
*Inorg. Chem.* 2015, 54, 7264−7271

(4) Hughes, H.; Allix, M. M. B.; Bridges, C. A.; Claridge, J. B.; Kuang, X.; Niu, H.; Taylor, S.; Song, W.; Rosseinsky, M. J. *J. Am. Chem. Soc.* **2005**, *127*, 13790−13791.
(5) Bridges, C. A.; Allix, M.; Suchomel, M. R.; Kuang, X.; Sterianou, I.; Sinclair, D. C.; Rosseinsky, M. J. *Angew. Chem., Int. Ed.* **2007**, *46*, 8785−8789.
(6) Tang, C. C.; Zhan, W. S.; Li, Y. X.; Chen, D. F.; Du, J.; Wu, G. H.; Gan, Z. W.; Qi, S. R. *J. Phys. D: Appl. Phys.* **1998**, *31*, 2426−2430.
(7) Hill, P. M.; Peiser, H. S.; Rait, J. R. *Acta Crystallogr.* **1956**, *9*, 981−986.
(8) Karunadasa, H.; Huang, Q.; Ueland, B. G.; Lynn, J. W.; Schiffer, P.; Regan, K. A.; Cava, R. J. *Phys. Rev. B: Condens. Matter Mater. Phys.* **2005**, *71*, 144414−1.
(9) Hirose, K.; Doi, Y.; Hinatsu, Y. *J. Solid State Chem.* **2009**, *182*, 1624−1630.
(10) Chern, G.; Perkins, N. *Phys. Rev. B: Condens. Matter Mater. Phys.* **2009**, *80*, 220405(4)(R).
(11) Niazi, A.; Bud'ko, S. L.; Schlagel, D. L.; Yan, J. Q.; Lograsso, T. A.; Kreyssig, A.; Das, S.; Nandi, S.; Goldman, A. I.; Honecker, A.; McCallum, R. W.; Reehuis, M.; Pieper, O.; Lake, B.; Johnston, D. C. *Phys. Rev. B: Condens. Matter Mater. Phys.* **2009**, *79*, 104432(21).
(12) Sakurai, H.; Irizawa, A.; Nanba, T. *J.Phys.: Conf.Ser.* **2012**, *344*, 012013/1.
(13) Sakurai, H. *Phys. Rev. B: Condens. Matter Mater. Phys.* **2008**, *78*, 094410(10).
(14) Yamaura, K.; Arai, M.; Sato, A.; Karki, A. B.; Young, D. P.; Movshovich, R.; Okamoto, S.; Mandrus, D.; Takayama-Muromachi, E. *Phys. Rev. Lett.* **2007**, *99*, 196601(4).
(15) Nozaki, H.; Sugiyama, J.; Månsson, M.; Harada, M.; Pomjakushin, V.; Sikolenko, V.; Cervellino, A.; Roessli, B.; Sakurai, H. *Phys. Rev. B: Condens. Matter Mater. Phys.* **2010**, *81*, 100410(4).
(16) Takahashia, Y.; Kataoka, K.; Ohshima, K.; Kijima, N.; Awaka, J.; Kawaguchi, K.; Akimoto, J. *J. Solid State Chem.* **2007**, *180*, 1020−1027.
(17) Akimoto, J.; Takei, H. *J. Solid State Chem.* **1989**, *79*, 212−217.
(18) Geselbracht, M. J.; Noailles, L. D.; Ngo, L. T.; Pikul, G. H.; Walton, R. I.; Cowell, E. S.; Millange, F.; O'Hare, D. *Chem. Mater.* **2004**, *16*, 1153−1159.
(19) Månsson, M.; Umegaki, I.; Nozaki, H.; Higuchi, Y.; Kawasaki, I.; Watanabe, I.; Sakurai, H.; Sugiyama, J. *arXiv.org, e-Print Archive, Cond. Mater.* **2014**, 1−6.
(20) Viciu, L.; Huang, Q.; Morosan, E.; Zandbergen, H. W.; Greenbaum, N. I.; McQueen, T.; Cava, R. J. *J. Solid State Chem.* **2007**, *180*, 1060−1067.
(21) Larson, A.; Von Dreele, R. B. *GSAS: Generalized Structure Analysis System*; Los Alamos National Laboratory, Los Alamos, NM, 1994.
(22) Reid, A. F.; Wadsley, A. D.; Sienko, M. J. *Inorg. Chem.* **1968**, *7*, 112−118.
(23) Shannon, R. D. *Acta Crystallogr., Sect. A: Cryst. Phys., Diffr., Theor. Gen. Crystallogr.* **1976**, *A32*, 751−767.
(24) Decker, B. F.; Kasper, J. S. *Acta Crystallogr.* **1957**, *10*, 332−337.
(25) Brese, N. E.; O'Keeffe, M. *Acta Crystallogr., Sect. B: Struct. Sci.* **1991**, *47*, 192−197.
(26) de Vries, M. A.; Mclaughlin, A. C.; Bos, J.-W. G. *Phys. Rev. Lett.* **2010**, *104*, 177202(4). de Vries, M. A.; Piatek, J. O.; Misek, M.; Lord, J. S.; Rønnow, H. M.; Bos, J.-W. G. *New J. Phys.* **2013**, *15*, 43024.
(27) Mclaughlin, A. C.; de Vries, M. A.; Bos, J.-W. G. *Phys. Rev. B: Condens. Matter Mater. Phys.* **2010**, *82*, 43024.


DOI: 10.1021/acs.inorgchem.5b00655
*Inorg. Chem.* 2015, 54, 7264−7271